Direct Numerical Simulation of Inverted Flag

Author

Hafiz Muhammad Umar

Regn Number

00000203661

Supervisor

Dr. Emad Uddin

DEPARTMENT OF MECHANICAL ENGINEERING

SCHOOL OF MECHANICAL & MANUFACTURING ENGINEERING

NATIONAL UNIVERSITY OF SCIENCES AND TECHNOLOGY

ISLAMABAD

SEPTEMBER, 2019

Direct Numerical Simulation of Inverted Flag

Author

Hafiz Muhammad Umar

Regn Number

00000203661

A thesis submitted in partial fulfillment of the requirements for the degree of

MS Mechanical Engineering

Thesis Supervisor:

Dr. Emad Uddin

Thesis Supervisor's Signature:

_____

DEPARTMENT OF MECHANICAL ENGINEERING

SCHOOL OF MECHANICAL & MANUFACTURING ENGINEERING

NATIONAL UNIVERSITY OF SCIENCES AND TECHNOLOGY,

ISLAMABAD

SEPTEMBER, 2019

THESIS ACCEPTANCE CERTIFICATE

Certified that final copy of MS thesis written by Mr. Hafiz Muhammad Umar Registration No. 2017-MS-ME-00000203661 of **SMME** has been vetted by undersigned, found complete in all aspects as per NUST Statutes/Regulations, is free of plagiarism, errors, and mistakes and is accepted as partial fulfillment for award of MS/MPhil degree. It is further certified that necessary amendments as pointed out by GEC members of the scholar have also been incorporated in the said thesis.

Signature with stamp: _____

Name of Supervisor: _____

Date: _____

Signature of HoD with stamp: _____

Date: _____

Countersign by

Signature (Dean/Principal): _____

Date: _____

Declaration

I certify that this research work titled "*Direct Numerical Simulation of Inverted Flag"* is my own work. The work has not been presented elsewhere for assessment. The material that has been used from other sources it has been properly acknowledged / referred.

Signature of Student

Hafiz Muhammad Umar

2017-NUST-MS-ME-00000203661

Language Correctness Certificate

This thesis has been read by an English expert and is free of typing, syntax, semantic, grammatical and spelling mistakes. Thesis is also according to the format given by the university.

Signature of Student
Hafiz Muhammad Umar
Registration Number
MS-ME-00000203661

Signature of Supervisor

Plagiarism Certificate (Turnitin Report)

This thesis has been checked for Plagiarism. Turnitin report endorsed by Supervisor is attached.

Signature of Student

Hafiz Muhammad Umar

Registration Number

2017-NUST-MS-ME-00000203661

Signature of Supervisor

Copyright Statement

Acknowledgements

I am thankful to my Creator ALLAH Subhanahu-Watala to have guided me throughout this work at every step and for every new thought which You setup in my mind to improve it. Indeed, I could have done nothing without Your priceless help and guidance. Whosoever helped me throughout the course of my thesis, whether my parents or any other individual was Your will, so indeed none be worthy of praise but You.

I am profusely thankful to my beloved parents who raised me when I was not capable of walking and continued to support me throughout in every department of my life.

I would also like to express special thanks to my supervisor Dr. Emad Uddin for his help throughout my thesis and for Advanced Fluid Mechanics and Finite Element Method courses which he has taught me. I can safely say that I haven't learned any other engineering subject in such depth than the ones which he has taught.

I would also like to thank Dr. Zaib Ali, Dr. Samiur Rahman Shah and Dr. Ali Zaidi for being on my thesis guidance and evaluation committee and express my special thanks them for their support and cooperation.

Finally, I would like to express my gratitude to all the individuals who have rendered valuable assistance to my study.

Dedicated to my exceptional parents and adored siblings whose tremendous support and cooperation led me to this wonderful accomplishment.

Abstract

The flapping motion of an inverted flag having free leading edge and clamped trailing edge behind the bluff body were simulated using the penalty immersed boundary method in a two-dimensional viscous flow. Three parameters were optimized, the Reynold's number (Re), bending rigidity (γ) and the streamwise gap (G_x) from the bluff body. These parameters were discussed with flapping modes, flapping amplitude, the power spectra and their vorticity interaction with flapping frequency. By placing the bluff body, the inverted flag showed three flapping modes; flapping mode, deflected mode and biased mode. Inverted flag in the flapping mode having high peak-to-peak amplitude (y/L) with high mean drag coefficient (C_d) is preferred for energy harvesting as it produces high strain energy (E_s). This happened for a finite range of flow speed or Re and γ at a far distance (G_x) from the bluff body. Critical Re and the range for γ was found in which flag flapped in the flapping mode keeping the mass ratio unity for all the simulations because, γ decides the bending momentum magnitude of the non-dimensionalized momentum equation of inverted flag. Vortices shed by the upstream bluff body had a strong effect on the flapping amplitude of downstream inverted flag. Lateral position of inverted flag and its effect on vorticity is discussed in detail with their power spectra to find the maximum amplitude and highest C_d. This research can help in concluding the optimum streamwise position of the inverted flag behind the bluff body.

Key Words: *Inverted Flag, Fluid structure interaction, Immersed boundary method, Critical Reynold's number*

Table of Contents

List of Figures

CHAPTER 1: INTRODUCTION

This research work has been done on the direct numerical simulation of a flexible inverted flag behind a bluff body. The objective was to find the critical Reynolds number (Re), bending rigidity coefficient (γ) and optimum streamwise gap (G_x) form bluff body by analyzing the phenomena involved between vortical structures produced by the bluff body and flexible flag. The scope of the research, previous work on conventional and inverted flexible structures in fluid flow, their numerical simulations and experimental studies are discussed in this chapter.

1.1 Scope, Background and Motivation

Due to the limited resources of fossil fuels, increase in demand and their environmental impacts, the search for harvesting energy from renewable resources is increased. In the recent years, most of the research has been done on flapping dynamics of flexible structures in a fluid flow and energy harvesting through it. Piezoelectric patches attached to the flexible structures can convert the strain energy caused by its deformation into electrical energy. The deformation can be from different sources, such as human motion, acoustic noise, fluttering flag, flapping birds etc. This is a kind of renewable energy resource. In nature, specially the aquatic animals like, motion of fish in water behaves like a flexible structure in fluid flow effects the motion of other fish behind it because of their vorticity effect. To mimic this phenomenon, a thin flexible sheet in any fluid flow like water or air can cause the deformations in the sheet. These deformations can be used to generate electric current. A thin sheet is termed as a flexible flag.

The flexible flag can have two configurations. One having clamped leading edge and free trailing edge, termed as conventional flag, while the other having free leading edge and clamped trailing edge is termed as inverted flag. Both can flap in a uniform flow or behind the bluff body. There are two energy conversion process in this phenomenon. First the kinetic energy of the fluid flow is converted into the strain energy of the flag, second this strain energy stored in the flag is converted into electrical energy through piezoelectric patches attached on its surface (Allen and Smits 2001, Michelin and Doaré 2013). Energy can be harvested from water or air flow to power

small devices like sensors or actuators at such places that are difficult to access, such as in deep oceans or in biofluid flows (Akcabay and Young 2012).

1.1.1 Conventional Flag

An upstream bluff body was placed with downstream conventional flag and their interaction was observed to optimize the energy harvesting technique and piezo electric material's efficiency. Many researchers tried to improve the energy harvesting efficiency by placing bluff body (Taylor, Burns et al. 2001, Zhang and Wang 2016).

Different configurations with conventional and inverted flag were used by many researchers to induce large oscillations and flapping amplitude like tandem, side by side and multiple flags in diamond or X-shaped arrangement. Downstream bodies are strongly influence by the vortices shed by and upstream body. Vorticity interaction with downstream flexible flag in tandem arrangement using conventional configuration was examined including the bending coefficient, frequency, phase angle and flapping amplitude of pitching and heaving motion. It was observed that the drag coefficient of the downstream flag was only slightly dependent on the gap distance between the two flags (Uddin, Huang et al. 2015).

Coupling performance of two identical flags in side-by-side (Xia, Doaré et al. 2016), parallel, tandem and staggered positions was studied in detail. Significant drag reductions were observed in the in-phase flapping mode for relatively small separation in parallel position (Sun, Wang et al. 2016). The interaction between conventional flexible flag and uniform flow in triangular, diamond and conical formations were investigated as a function of both bending coefficients and gap distance between the flag (Uddin, Huang et al. 2013).

1.1.2 Inverted Flag

Flow velocity can be increased to induce large deformations in the flag, which increases the energy harvesting efficiency (Michelin and Doaré 2013). In most studies, an upstream bluff body was used additionally to enlarge vorticity effect on the downstream flexible structure. This

helped in inducing large oscillations in the flag and become unstable at low critical flow velocity providing high flapping amplitude (Kim, Kang et al. 2017).

The configuration of our interest was an inverted flag with free leading edge and clamped trailing edge behind an upstream bluff body. The concept of inverted flag was mimicked by flapping leaves due to the air passing through it (Shao, Chen et al. 2012). This is the fact that a mechanical model with free front end and clamped rear end is generally more unstable to external axial loading than a clamped front end and a free rear end. An inverted flag had high flapping amplitude and stored large strain energy due to unsteady drag force (Kim, Cossé et al. 2013).

1.1.2.1 Inverted Flag in a Uniform Flow

(Kim, Cossé et al. 2013) studied the flapping dynamics of a thin sheet in inverted configuration to observe its stability effected by parameters like bending rigidity, free stream velocity, density and flexible sheet length. It was found that for the instability of inverted flag, mass ratio was not an important factor. (Orrego, Shoele et al. 2017) experimentally conducted the parametric study to evaluate the effect of geometrical parameters of an inverted flag on the flapping behavior and energy output. They also harvested ambient wind energy ($\sim 0.4\ Wcm^{-3}$) even at low wind speed regimes ($\sim 3.4\ ms^{-1}$) to power a temperature sensor. It was demonstrated that high aspect and mass ratio of inverted flag able to harvest high electrical power due to higher bending curvatures and faster flapping frequencies.

(Tang, Liu et al. 2015) numerically studied the dynamics of inverted flexible sheet in uniform flow. Flapping modes, effects of the mass ratio, inclination angle, the Reynolds number (Re), elastic strain energy and vortical structures around the plate were discussed in detail. (Ryu, Park et al. 2015) examined the vortical structures and flapping dynamics of inverted flag in a uniform flow in terms of bending rigidity (γ) and the Reynolds number. It was concluded that peak-to-peak amplitude influenced the dynamics of inverted flag and its energy harvesting efficiency. As the maximum strain energy was obtained near the trailing edge so, piezoelectric patches to be attached as close as possible near the trailing edge.

1.1.2.2 Inverted Flag with Multiple Arrangement

(Shoele and Mittal 2016) coupled the piezoelectric mechanism with inverted flag in a uniform flow followed by comprehensive study on the effects of bending rigidity, flag inertia and Reynolds number with vortical structures. (Kim, Kang et al. 2017) experimentally investigate the dynamics of two types of downstream flag, a conventional and an inverted flag, on and off a midline behind an upstream bluff body in water and air flows. Maximum flapping amplitude reached by the inverted flag behind the bluff body was almost constant and the flapping behavior in both water and air flow was similar. An inverted flag behind the bluff body showed sharp transition to the large amplitude at certain free-stream velocity of 2.8 when the flag is far from the bluff body at G_x 1.67 and 2.00. Like conventional flag, simulations on inverted flag in a uniform flow were carried out for side by side arrangement to study the flapping dynamics, flag properties in dimensionless parameters and spanwise gap distance between them (Huertas-Cerdeira, Fan et al. 2018, Ryu, Park et al. 2018).

1.1.2.3 Inverted Flag Behind a Bluff Body

To the best of author's knowledge, little information is available on the flapping behavior of an inverted flag behind the bluff body, specifically its numerical analysis was not performed yet. The objective of this study was to explore the dynamics of an inverted flag behind the bluff body using penalty immersed boundary method, such that vortical structures generated by the bluff body can be examined to improve the efficiency of an energy harvesting system, likewise when an upstream bluff body was placed with conventional flag. The parametric study was carried out to find the critical Reynolds number (Re) and streamwise gap (G_x) from bluff body in terms of binding rigidity (γ) so that the maximum amplitude with high coefficient of drag (C_d) may be achieved which could be responsible for greater energy harvesting than an inverted flag in a uniform flow. The underlying phenomena involved in different vortex shedding and frequency modes are also discussed in detail.

CHAPTER 2: ANALYTICAL MODEL AND NUMERICAL SCHEME

Study of flexible structure in a uniform flow to analyze the material changes is a fluid structure interaction problem. A flexible flag in a uniform flow was modeled using immersed boundary method to solve the structural equations. Problem formulation and methodology to solve the whole scheme is discussed in detail in this chapter.

2.1 Problem Formulation and Methodology

A flexible structure with free leading edge and a fixed trailing edge called an inverted flag behind a bluff body was modeled in a 2D viscous fluid flow having free stream velocity of U_∞ as shown in the schematic diagram of figure 1. L is the characteristic length of inverted flag with origin of coordinate system at the fixed edge. Dashed curved lines shown the instantaneous position of flag in flapping mode. G_x is the streamwise gap from bluff body to the fixed trailing edge of the flag.

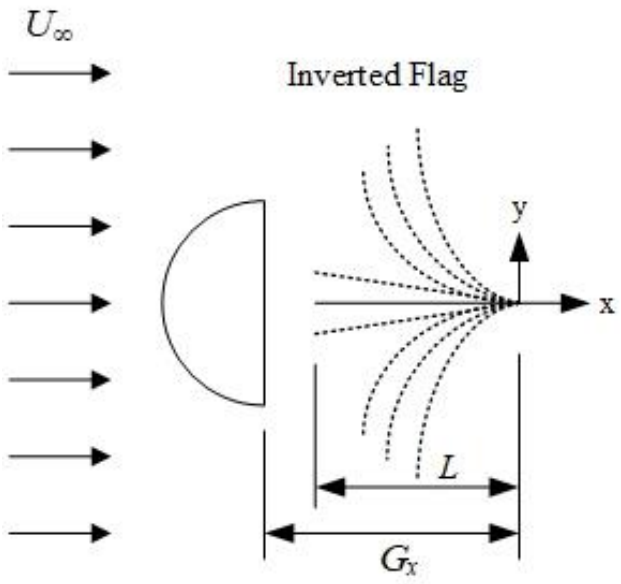

FIGURE 1: Schematic diagram of an inverted flag behind the bluff body

Systems involving flexible structures interacting with the surrounding fluid are common in nature and became challenging to model because of complex geometries and complicated fluid dynamics. The fluid exerts force on the flexible structure due to the pressure difference and viscous shear stresses causes it to move with the fluid. The system was modeled using the Penalty

Immersed Boundary Method (PIBM) which was an improved version of Immersed boundary method (IBM) first used in reference to a method developed by (Peskin 1972) to handle the interaction between flexible structure and a uniform flow in which the momentum forcing was added to the Navier-Stokes equation. This method has great advantage due to its simplified grid generation requirements (Mittal and Iaccarino 2005). In this method the flexible structure was imaginarily be decomposed into a massive and massless part. The massive part is the only part on which the elastic force was exerted, which is the Lagrangian force which can be derived by the principle of virtual work or a constitutive law such as Hooke's Law (Peskin 2002) and the massless part interacted with the local fluid velocity. Both are connected with stiff spring as shown in figure 2 (Kim and Peskin 2007). PIBM can handle the mass of the flag also, as the mass of the flexible structure plays a significant role in flapping dynamics, that cannot be neglected and can solve the cases in which the structure or immersed boundary has greater mass than that of the fluid it displaces (Kim, Baek et al. 2002).

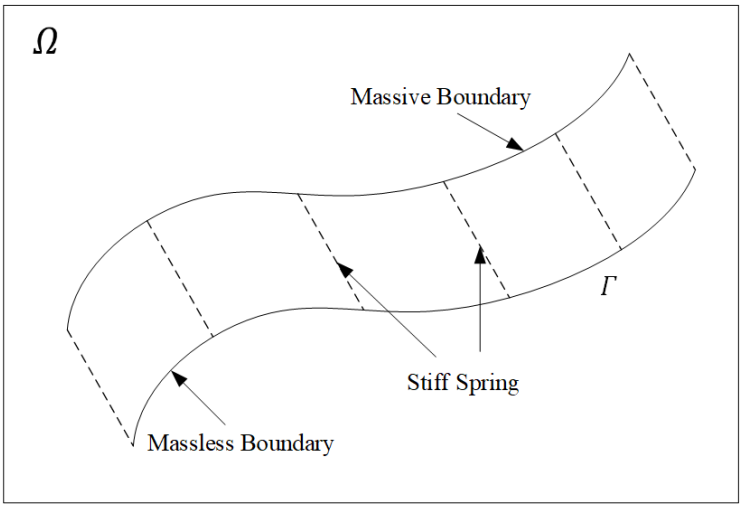

FIGURE 2: Stiff Spring connection between massive and massless boundaries

The fluid domain Ω was modeled in fixed Eulerian cartesian mesh and flexible structure was modeled on freely moving Lagrangian coordinates having immersed boundary Γ. The fluid flow was governed by Navier-Stokes and continuity equations.

$$\rho_o \left(\frac{\partial \boldsymbol{u}}{\partial t} + \boldsymbol{u} \cdot \nabla \boldsymbol{u} \right) = -\nabla p + \mu \nabla^2 \boldsymbol{u} + \boldsymbol{f} \tag{1}$$

$$\nabla \cdot \boldsymbol{u} = 0 \tag{2}$$

Where ρ_0 is the fluid density, $\boldsymbol{u} = (u, v)$ is the velocity vector, p is the pressure, μ is the dynamic viscosity and $\boldsymbol{f} = (f_x, f_y)$ is the momentum forcing used to enforce the no-slip boundary conditions along the immersed boundary. Fluid equations were solved by fractional step method (Kim, Baek et al. 2002) with a staggered cartesian grid system.

The structural equations were solved by iterative scheme of finite difference method to calculate solid motion equations. More details of the numerical schemes can be found in (Huang, Shin et al. 2007). The flag position $X = X(s, t)$ was governed by the equation:

$$\rho_1 \frac{\partial^2 \boldsymbol{X}}{\partial t^2} = \frac{\partial}{\partial s}\left(T \frac{\partial \boldsymbol{X}}{\partial s}\right) - \frac{\partial^2}{\partial s^2}\left(\gamma \frac{\partial^2 \boldsymbol{X}}{\partial s^2}\right) - \boldsymbol{F} \tag{3}$$

Where ρ_1 is the density difference between the fluid and the flexible flag, s is the arc length, $\boldsymbol{T}$ is the tension force along the axis of flag, γ is the bending rigidity coefficient and $\boldsymbol{F}$ is the Lagrangian forcing exerted on the flag by the fluid flow. Equations (2) – (3) were non-dimensionalized using various characteristic scales. The fluid density ρ_0 was used for normalizing the density, the free stream velocity U_∞ for the velocity, the characteristic length L of flexible inverted flag for length, L/U_∞ for time, $\rho_0 U_\infty^2$ for pressure p, $\rho_1 U_\infty^2$ for tension force $\boldsymbol{T}$, $\rho_1 U_\infty^2 / L$ for the momentum forcing exerted by the flexible flag on the fluid $\boldsymbol{f}$ and $\rho_1 U_\infty^2 L^2$ for bending rigidity coefficient γ (Huang, Shin et al. 2007). γ is non-dimensional bending rigidity coefficient, is a function of Young's modulus (E) and the second moment of area (I) of the flexible structure explained by (Rominger and Nepf 2014). Equations (1) – (3) converted into following non-dimensionalized form:

$$\frac{\partial \boldsymbol{u}}{\partial t} + \boldsymbol{u} \cdot \nabla \boldsymbol{u} = -\nabla p + \frac{1}{Re} \nabla^2 \boldsymbol{u} + \boldsymbol{f}$$

$$\frac{\partial^2 \boldsymbol{X}}{\partial t^2} = \frac{\partial}{\partial s}\left(\boldsymbol{T} \frac{\partial \boldsymbol{X}}{\partial s}\right) - \frac{\partial^2}{\partial s^2}\left(\gamma \frac{\partial^2 \boldsymbol{X}}{\partial s^2}\right) - \boldsymbol{F}$$

Where, $Re = \rho U L / \mu$ is a non-dimensional Reynolds number. The tension force $\boldsymbol{T}$ can be calculated using the inextensibility condition of flexible flag. The IBM did not strictly satisfied the inextensibility condition of the flexible structure, which were solved in PIBM (Huang, Shin et al. 2007) and is expressed by:

$$\frac{\partial \boldsymbol{X}}{\partial s} \cdot \frac{\partial \boldsymbol{X}}{\partial s} = 1$$

The boundary conditions applied at the clamped trailing edge of the flexible structure ($s = 0$) $as\ X_0 = (0,0)$ were;

$$\boldsymbol{X} = \boldsymbol{X}_0 \quad , \quad \frac{\partial \boldsymbol{X}}{\partial s} = (-1,0)$$

At the free leading edge ($s = L$), therefore;

$$\boldsymbol{T} = 0 \quad , \quad \frac{\partial^2 \boldsymbol{X}}{\partial s^2} = (0,0) \quad , \quad \frac{\partial^3 \boldsymbol{X}}{\partial s^3} = (0,0)$$

2.1.1 Fluid Structure Interaction

The fluid flow and the flexible structure motions, i.e., cartesian and curvilinear computational meshes do not coincide (Kim and Peskin 2007), and solved separately in each coordinate system and their interaction were calculated using a feedback force of momentum forcing F. As the penalty immersed boundary method includes the mass of the flexible structure. The immersed boundary was split into two Lagrangian components. Massless component interacted with fluid in the same way as in IBM, it moved at the local fluid velocity and applied local force on the fluid. The other massive component connected to massless component by a system of stiff springs with damping. (Lai and Peskin 2000) used a stiff spring restoring force to force the immersed boundary to attach to the equilibrium or prescribed positions. Their separation is inversely proportional to the stiffness of spring (Kim and Peskin 2007) but both components moved together, that's why both velocities were equal, ensuring no-slip boundary condition on the surface of inverted flag. The momentum forcing was obtained on the Lagrangian grid using equations of motion for structure and spread to the nearby Eulerian grids by smoothed approximation of the Dirac delta function. The momentum forcing term was obtained by the following relation:

$$\boldsymbol{F} = \alpha \int_0^t (\boldsymbol{U}_{ib} - \boldsymbol{U}) dt' + \beta (\boldsymbol{U}_{ib} - \boldsymbol{U})$$

Where α and β are large negative free constants set to be -10^5 and -10^2 respectively calculated by (Huang, Shin et al. 2007), $\boldsymbol{U}_{ib}$ is the fluid velocity on the immersed boundary obtained by interpolation, $\boldsymbol{U}$ is the velocity of inverted flag calculated by $\boldsymbol{U} = d\boldsymbol{X}/dt$ and dt is the time step for simulation. After calculating the Lagrangian momentum forcing term F, it transformed to f in the Eulerian grid using smoothed Dirac delta function and fluid velocity expressed as:

$$\boldsymbol{U}_{ib}(s,t) = \int_{\Omega} \boldsymbol{u}(\boldsymbol{x},t)\delta(\boldsymbol{X}(s,t) - \boldsymbol{x})d\boldsymbol{x}$$

While the momentum forcing appeared to be:

$$\boldsymbol{f}(\boldsymbol{x},t) = \rho \int_{\Gamma} \boldsymbol{F}(s,t)\delta(\boldsymbol{x} - \boldsymbol{X}(s,t))ds$$

Where, Ω is the fluid domain, Γ is the immersed boundary domain, δ is a two-dimensional Dirac delta function but having only one integral ds and ρ is the density ratio, which was non-dimensionalized by $\rho_1/\rho_0 L_r$. In the present study, we set $\rho = 1$ means that the density of inverted flag is same as that of fluid density.

2.1.2 Iterative Scheme of Numerical Method

In short, the whole numerical iterative scheme for the solution of fluid-structure interaction can be summarized as follow:

1. Initialize the computational parameters, the mesh grids, the fluid and flexible structure motion by setting $\boldsymbol{X}_{ib}^0 = \boldsymbol{X}^0$, $\boldsymbol{U}_{ib}^0 = \boldsymbol{U}^0$ where, $\boldsymbol{X}_{ib}^0$, $\boldsymbol{U}_{ib}^0$ is the position and velocity of immersed boundary at time 0 respectively.
2. At the nth time step, the fluid velocity $\boldsymbol{u}^n$, the position of flexible structure $\boldsymbol{X}^n$ and $\boldsymbol{X}^{n-1}$ and the velocity $\boldsymbol{U}^n$ are known. Interpolate the fluid velocity at the Lagrangian points of IB to obtain $\boldsymbol{U}_{ib}^n$, then calculate the Lagrangian interaction force $\boldsymbol{F}^n$
3. Spread the Lagrangian force $\boldsymbol{F}^n$ on the Eulerian grid to obtain the updated fluid velocity field and the pressure field.
4. To obtain the flexible structure position at the new time step $\boldsymbol{X}^{n+1}$; Calculate the tension force $\boldsymbol{T}$ at the intermediate time step $\boldsymbol{T}^{n+1/2}$ by substituting $\boldsymbol{F}^n$ into the flag

position as well as the fluid velocity $\boldsymbol{U}^{n+1} = (\boldsymbol{X}^{n+1} - \boldsymbol{X}^{n})/\Delta t$. One step marching is completed, now return to the step 2 and calculate the values for next time step.

2.1.3 Computational Domain

In this simulation, rectangular computational domain for fluid-structure interaction was chosen in which uniform flow flows from left to right as shown in Fig. 1 ranged from (-2, 6) in the streamwise x direction and (-4, 4) in the spanwise y direction. Both directions were normalized by length of flag (L). The Eulerian grid size set for the fluid was (512×350) in the streamwise and spanwise directions respectively and the Lagrangian grid size for flag was 64. The Eulerian grid was uniformly distributed along the streamwise x direction, and uniform in the y direction for (-2 ≤ y ≤ 2) but stretched otherwise. Dirichlet boundary conditions ($u = U_{\infty}, v = 0$) were applied at the inlet, top and bottom walls of fluid domain. And the convective boundary conditions were used at the outlet of the fluid domain.

The computational time step was set to be 5×10^{-5}, which resulted in CFL number of 0.1. Complete procedure, validation of flow solver for immersed boundary method as well as the structure motion of flag is discussed in details by (Huang, Shin et al. 2007). The initial position of the flag called the inclination angle was 0 or in parallel to the streamwise flow direction. The flow dynamics was investigated for 200 flapping periods. The flow patterns were characterized by the mean drag coefficient C_d, the amplitude of tail position, the power spectrum and the vorticity contours. Three parameters were optimized, the Reynold's number Re, bending rigidity coefficient γ and the streamwise gap distance G_x. These parameters were discussed with flapping modes, flapping amplitude, the power spectrum and their vorticity effect.

CHAPTER 3: RESULTS AND DISCUSSION

This chapter covers the results obtained from simulation performed on the bases of methodology discussed in chapter 2. First the critical Reynold's number (Re) is found than bending rigidity (γ) is finalized. The streamwise gag (G_x) is also varied to get the optimum position of flag. Lateral position of leading edge (y/L) with its effect on vorticity and their Fourier transform is discussed in detail in this chapter.

3.1 Results

Inverted flag produce more mean strain energy than the conventional flag because of high peat-to-peak amplitude (A/L) and bending rigidity (γ) (Ryu, Park et al. 2015) due to high instabilities. In the present study, oscillations in an inverted flag were induced by vortices shed from an upstream bluff body as shown in Fig. 1. By placing an upstream bluff body; the flapping behavior of the downstream flag changes because of increase in instabilities, As the bluff body continuously sheds alternating vortices with varying size and frequency depends upon its geometry and the free stream velocity. So, the fluid flow and structural parameters totally change. The first most important task was to finalize the parameters like, Reynold's number Re, and bending rigidity γ keeping the mass ratio unity for all the simulations because the bending rigidity decides the bending momentum magnitude of the non-dimensionalized momentum equation of inverted flag. The results were compared with (Kim, Cossé et al. 2013, Ryu, Park et al. 2015, Sader, Cossé et al. 2016, Kim, Kang et al. 2017).

3.1.1 Critical Reynold's Number

Critical Reynold's number (Re) can be defined here at which flag flap smoothly in the flapping mode. Re and bending rigidity (γ) were varied for the fixed streamwise position $G_x = 1$ which could be the minimum gap from the bluff body and observed that there is a small range for these parameters in which continuous flapping occur. Flapping was found to be $0.005 \leq \gamma \geq 0.01$. Two flapping modes were found; the flapping mode and the deflected mode. for $Re \leq 50$

deflected mode with small flapping amplitude, for $100 \leq Re \geq 150$ flapping mode and for $Re \geq 175$ high amplitude deflected mode. Solution started diverging at $Re \geq 300$ and for $\gamma > 0.01$. For $Re \leq 50$ the straight mode and flapping mode did not occur because of two reason, one, the bluff body continuously shed vortices which deformed the flag, second, the viscous forces were dominating the inertial forces. The results followed the pattern as observed by (Ryu, Park et al. 2015); as Re increases with the increase of γ, flapping modes shifted from deflected to flapping mode, remained in flapping mode within certain range of Re and γ, then shifted towards the biased mode.

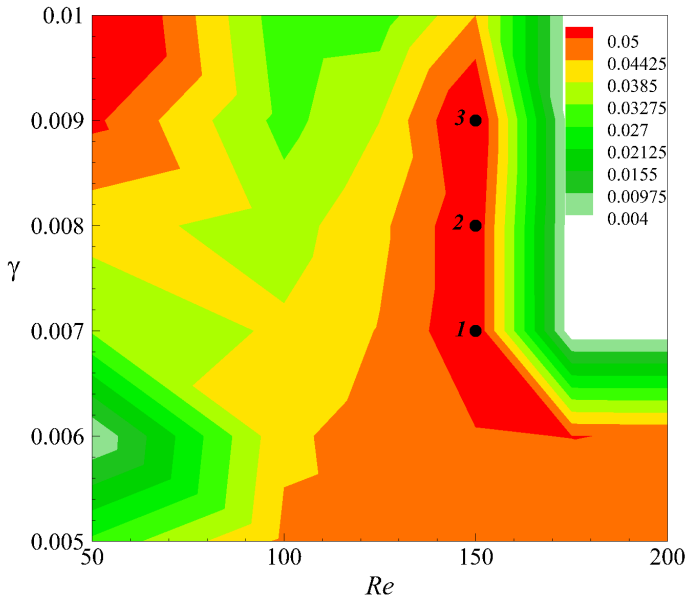

FIGURE 3: Contours of Mean drag coefficient (C_d) for varying Re and bending rigidity (γ)

Mean drag coefficient (C_d) increased as the Reynold's number (Re) increased with the increase in bending rigidity (γ) as shown in Figure 3. Large drag force with large peak-to-peak flapping amplitude could lead to large energy harvesting. Highest mean drag coefficient C_d was found at three points 1 – 3. They have almost same C_d but a little bit difference in maximum amplitude. At point 2; $Re = 150, \gamma$ = 0.008 has highest flapping amplitude with high C_d. Power spectrum in Figure 4 (b) is showing that it has smooth flapping also. Solution started diverging $0.005 < \gamma > 0.01$ for So, $Re = 150$ was finalized as critical for smooth flapping with highest C_d and flapping amplitude and the range for bending rigidity γ was set to be $0.005 - 0.01$.

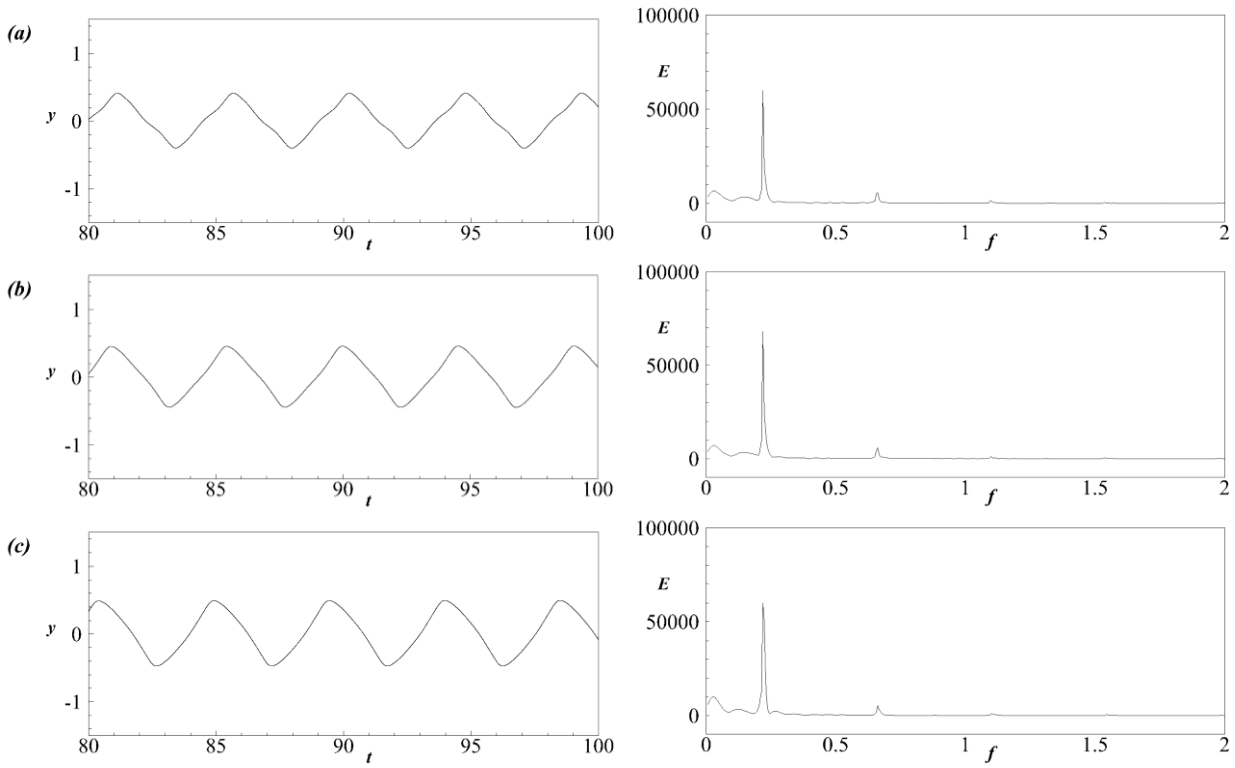

FIGURE 4: Amplitude and Frequency plots for $Re = 150$ at (a) γ = 0.007 (b) γ = 0.008 (c) γ = 0.009

3.1.2 Variation of Streamwise Distance

Streamwise distance G_x was varied from 1.0 – 3.0 for fixed $Re = 150$ with changing $\gamma = 0.005 - 0.01$. Three flapping modes were observed, flapping mode, deflected mode and the biased mode as shown in Figure 5. The straight mode did not occur as the bluff body continuously shed vortices which flapped the flag continuously. For $G_x = 1.1$; deflected mode, a wide range of flapping mode; $1.2 \leq G_x \geq 1.9$ except $G_x = 1.7$, an intermediate mode between flapping and deflected mode called the biased mode for $2.0 \leq G_x \geq 2.3$, again deflected mode for $G_x \geq 2.4$. The exception for $G_x = 1.7$ is because the vortex shedding frequency did not match the flapping of inverted flag at this gap. The deflected mode maintained the curved shape of inverted flag while, in biased mode, the curved shape did not maintain, it flapped in both flapping and deflected modes. In the flapping mode, inverted flag maintains almost same gap between mean position and extreme positions.

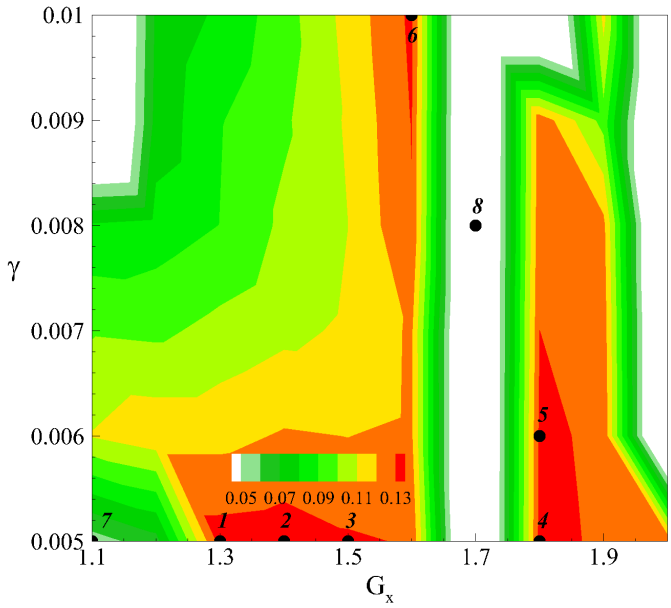

FIGURE 5: Contours for mean drag coefficient (C_d) with variation of streamwise gap (G_x)

Mean drag coefficient (C_d) first increased, reached maximum value than decreased as the streamwise gap (G_x) increased with the increase in bending rigidity (γ) as shown in mean drag coefficient contours figure as a function G_x and γ. Maximum C_d lie in the certain range of G_x. Contours for $G_x = 1.1 - 2.0$ were plotted which lie in the flapping mode because deflected mode is not beneficial for energy harvesting (Gurugubelli and Jaiman 2015). White region in figure 5 is showing the deflected mode within the range G_x plotted for. In general, six points with highest C_d, one with lowest C_d and one within deflected mode are discussed with lateral position of leading edge and vorticity contours in the next section.

3.1.3 Lateral position of Leading Edge and Vorticity Contours

Lateral position of inverted flag's leading edge (y/L) determines the maximum amplitude obtained during flapping. A high value of y/L corresponds to high bending of flag, which result in high bending energy and the chances of high strain energy (Ryu, Park et al. 2015). Large flapping amplitude with high C_d is preferred because it generates more bending energy (Gurugubelli and Jaiman 2015)**.** Figure 6 is showing the leading-edge positions of flag and instantaneous vortices with varying G_x and γ. Point A is the position of flag when it is at the top

extreme and point B for the lowest extreme position. For these two points A and B, vorticity interaction with flag is shown on the right side, in the frames A and B respectively.

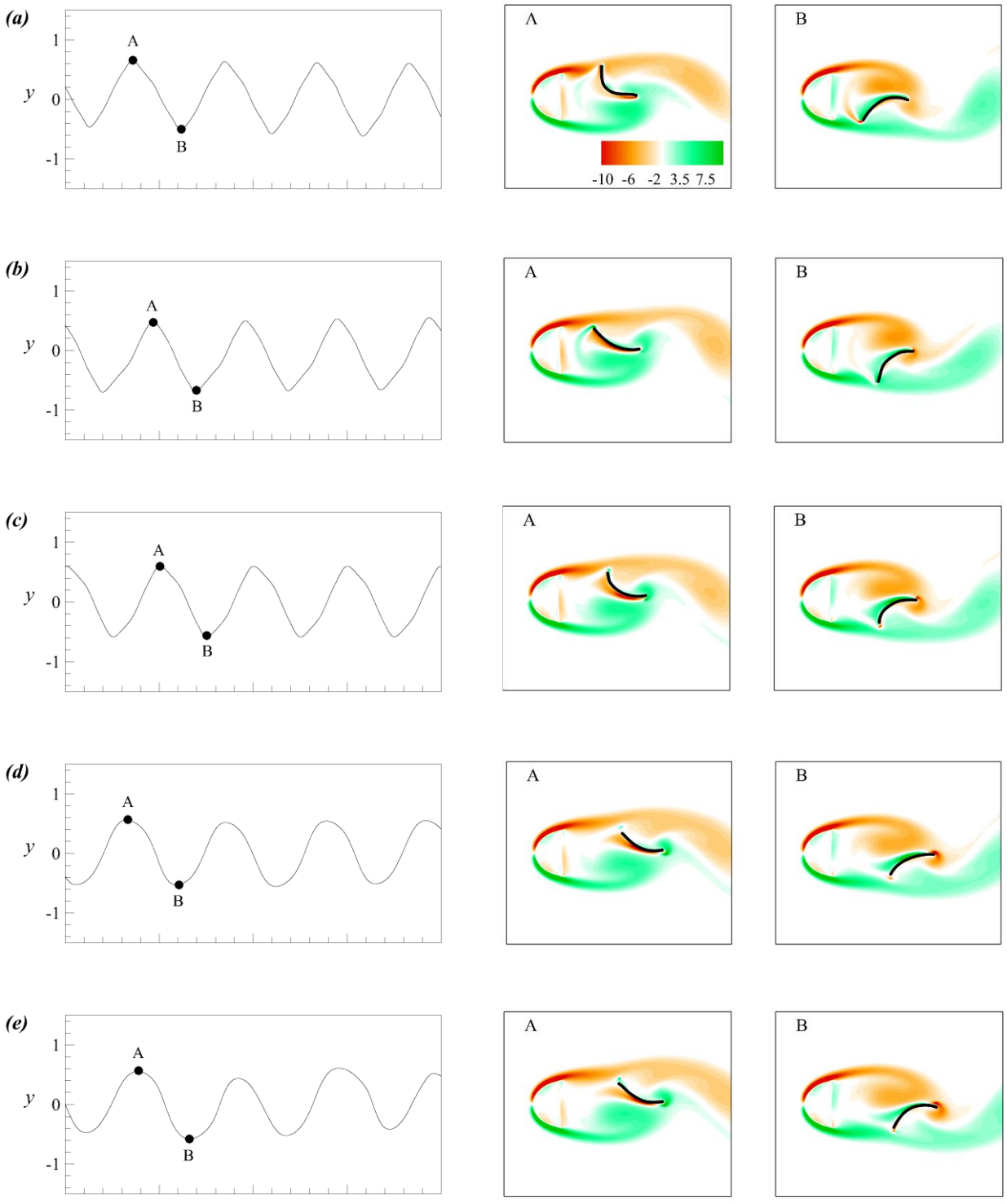

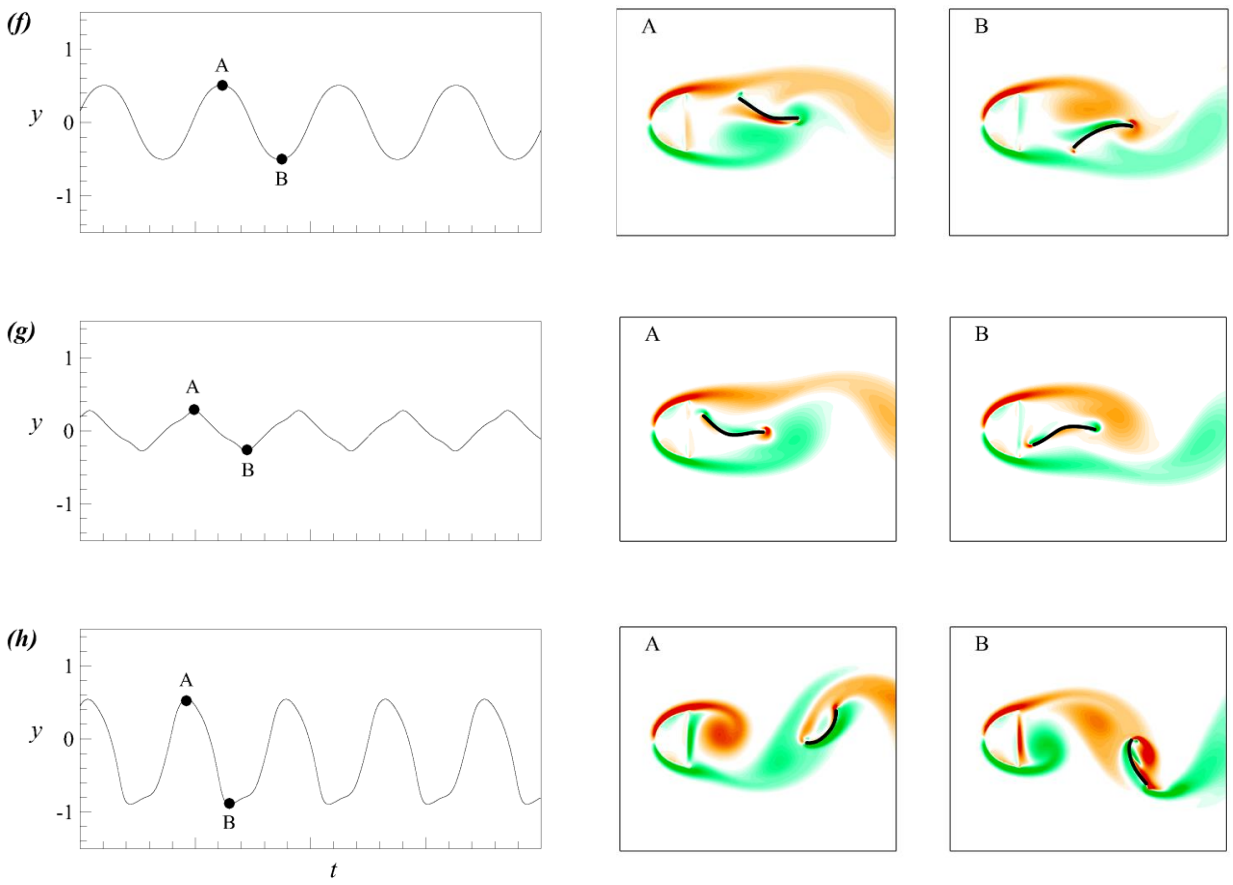

FIGURE 6: Flapping amplitude and Vorticity contours

Point 1 – 6 in Figure 5 that flapping amplitude first decreased than increased with the increase in G_x and γ. Also, the smoothness of flapping showed the same behavior within certain range of G_x because the vortex shedding frequency synchronized with flapping frequency of inverted flag. $G_x = 1.5$ (Point 3) has the high flapping amplitude with smooth flapping. An inverted flag behind a bluff body showed maximum flapping amplitude at certain gap $G_x = 1.67, 2.0$ (Kim, Kang et al. 2017) and for a finite band of flow speed (Sader, Cossé et al. 2016). At point 7; $G_x = 1.1, \gamma = 0.005$; flag has least peak-to-peak amplitude in figure (g) and significant drag reduction C_d in figure 5, as most of the flow passed the flag without touching it and flapped in the near wake of bluff body, also, non-uniform flow disturbs the stable state of downstream flag with irregular oscillations at low amplitude (Kim, Kang et al. 2017) but with the increase of γ, C_d also increased. At point 8; $G_x = 1.7$; highest flapping amplitude but in deflected mode and behaved like conventional flag in figure (h), so, this position is not suitable for energy harvesting. At this

position, larger upper vortex provided large momentum so, it deflected, further vortex shedding kept it in deflected mode. At $G_x \geq 1.7$ most of the cases vortex shedding frequency does not match properly. Power spectra of leading-edge positions for same frequency and varying G_x and γ for all the cases discussed previously in term of E are shown in figure 7. It gives the fundamental frequency of flapping which verified the results as discussed. Keeping in view the peak-to-peak amplitude and maximum C_d, $\gamma = 0.005$ provided more variation in streamwise distance G_x, with highest C_d.

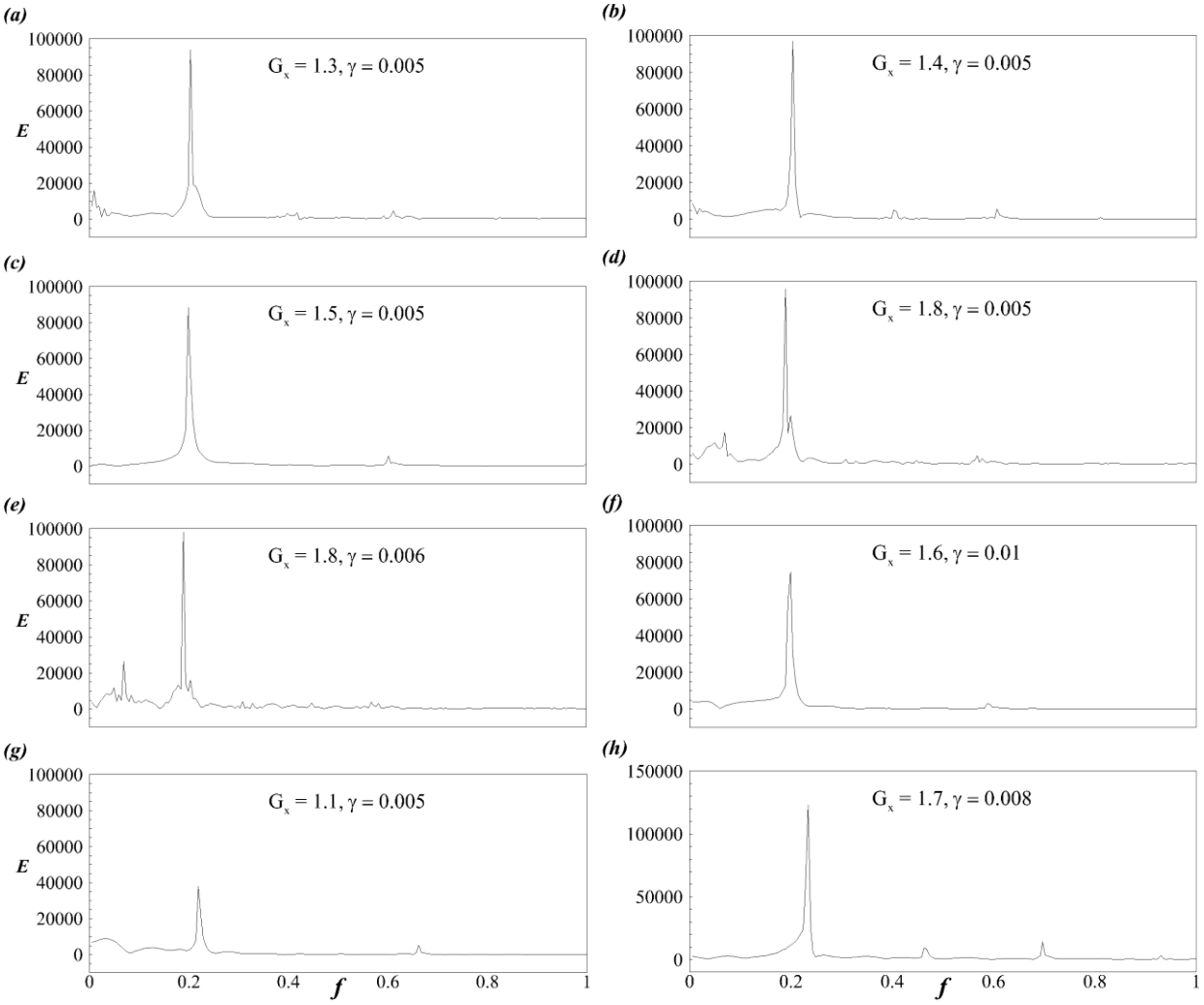

FIGURE 7: Power Spectra for varying G_x and γ in term of E

3.2 Conclusion

Direct numerical simulation of an inverted flag behind the bluff body was done using the immersed boundary method to investigate the excitation produced by vortex shedding of the bluff body. Critical Reynolds number (Re) and bending rigidity (γ) was found in which flag flapped continuously. Critical Re was found to be 150. The flapping dynamics and vortical structures around the inverted flag were examined in terms of γ and streamwise gap distance (G_x). Three types of flapping modes were found. $\gamma = 0.005$ provided more variations in G_x with highest coefficient of drag (C_d). It has been observed that with the increase in G_x, γ needs to be increased within the certain range. An inverted flag behind the bluff body flapped at high amplitude at specific streamwise gap and finite range of flow speed (Sader, Cossé et al. 2016, Kim, Kang et al. 2017). $G_x = 1.5$ has high and smooth flapping amplitude in all the cases analyzed as the vortex shedding interaction with flag flapping was synchronized. The power spectra verified the smoothness and high peak-to-peak flapping amplitude for the selected parameters. Mean drag coefficient (C_d) and elastic mean strain energy (E_s) have the same trend (Ryu, Park et al. 2015). So, it can be depicted that $G_x = 1.5$ with $\gamma = 0.005$ give high E_s. The spanwise gap distance (G_y) is needed to be varied to get the most optimum position of inverted flag behind the bluff body for maximum energy harvesting.

REFERENCES

1. Akcabay, D. T. and Y. L. Young (2012). "Hydroelastic response and energy harvesting potential of flexible piezoelectric beams in viscous flow." Physics of Fluids **24**(5): 054106.

2. Allen, J. and A. Smits (2001). "Energy harvesting eel." Journal of Fluids and Structures **15**(3-4): 629-640.

3. Gurugubelli, P. and R. Jaiman (2015). "Self-induced flapping dynamics of a flexible inverted foil in a uniform flow." Journal of Fluid Mechanics **781**: 657-694.

4. Huang, W.-X., et al. (2007). "Simulation of flexible filaments in a uniform flow by the immersed boundary method." Journal of Computational Physics **226**(2): 2206-2228.

5. Huertas-Cerdeira, C., et al. (2018). "Coupled motion of two side-by-side inverted flags." Journal of Fluids and Structures **76**: 527-535.

6. Kim, D., et al. (2013). "Flapping dynamics of an inverted flag." Journal of Fluid Mechanics **736**.

7. Kim, H., et al. (2017). "Dynamics of a flag behind a bluff body." Journal of Fluids and Structures **71**: 1-14.

8. Kim, K., et al. (2002). "An implicit velocity decoupling procedure for the incompressible Navier–Stokes equations." International journal for numerical methods in fluids **38**(2): 125-138.

9. Kim, Y. and C. S. Peskin (2007). "Penalty immersed boundary method for an elastic boundary with mass." Physics of Fluids **19**(5): 053103.

10. Lai, M.-C. and C. S. Peskin (2000). "An immersed boundary method with formal second-order accuracy and reduced numerical viscosity." Journal of Computational Physics **160**(2): 705-719.

11. Michelin, S. and O. Doaré (2013). "Energy harvesting efficiency of piezoelectric flags in axial flows." Journal of Fluid Mechanics **714**: 489-504.

12. Mittal, R. and G. Iaccarino (2005). "Immersed boundary methods." Annu. Rev. Fluid Mech. **37**: 239-261.

13. Orrego, S., et al. (2017). "Harvesting ambient wind energy with an inverted piezoelectric flag." Applied energy **194**: 212-222.

14. Peskin, C. S. (1972). "Flow patterns around heart valves: a numerical method." Journal of Computational Physics **10**(2): 252-271.

15. Peskin, C. S. (2002). "The immersed boundary method." Acta numerica **11**: 479-517.

16. Rominger, J. T. and H. M. Nepf (2014). "Effects of blade flexural rigidity on drag force and mass transfer rates in model blades." Limnology and oceanography **59**(6): 2028-2041.

17. Ryu, J., et al. (2015). "Flapping dynamics of an inverted flag in a uniform flow." Journal of Fluids and Structures **57**: 159-169.

18. Ryu, J., et al. (2018). "Flapping dynamics of inverted flags in a side-by-side arrangement." International Journal of Heat and Fluid Flow **70**: 131-140.

19. Sader, J. E., et al. (2016). "Large-amplitude flapping of an inverted flag in a uniform steady flow–a vortex-induced vibration." Journal of Fluid Mechanics **793**: 524-555.

20. Shao, C.-P., et al. (2012). "Wind induced deformation and vibration of a Platanus acerifolia leaf." Acta Mechanica Sinica **28**(3): 583-594.

21. Shoele, K. and R. Mittal (2016). "Energy harvesting by flow-induced flutter in a simple model of an inverted piezoelectric flag." Journal of Fluid Mechanics **790**: 582-606.

22. Sun, C., et al. (2016). "Force measurement on coupled flapping flags in uniform flow." Journal of Fluids and Structures **61**: 339-346.

23. Tang, C., et al. (2015). "Dynamics of an inverted flexible plate in a uniform flow." Physics of Fluids **27**(7): 073601.

24. Taylor, G. W., et al. (2001). "The energy harvesting eel: a small subsurface ocean/river power generator." IEEE journal of oceanic engineering **26**(4): 539-547.

25. Uddin, E., et al. (2013). "Interaction modes of multiple flexible flags in a uniform flow." Journal of Fluid Mechanics **729**: 563-583.

26. Uddin, E., et al. (2015). "Actively flapping tandem flexible flags in a viscous flow." Journal of Fluid Mechanics **780**: 120-142.

27. Xia, Y., et al. (2016). "Electro-hydrodynamic synchronization of piezoelectric flags." Journal of Fluids and Structures **65**: 398-410.

28. Zhang, M. and J. Wang (2016). "Experimental study on piezoelectric energy harvesting from vortex-induced vibrations and wake-induced vibrations." Journal of Sensors **2016**.